

1-2009

Physics of Carrier Backscattering in One- and Two-Dimensional Nanotransistors

Raseong Kim

Purdue University - Main Campus

Mark S. Lundstrom

School of Electrical and Computer Engineering, Birck Nanotechnology Center, Purdue University, lundstro@purdue.edu

Follow this and additional works at: <http://docs.lib.purdue.edu/nanopub>



Part of the [Nanoscience and Nanotechnology Commons](#)

Kim, Raseong and Lundstrom, Mark S., "Physics of Carrier Backscattering in One- and Two-Dimensional Nanotransistors" (2009).
Birck and NCN Publications. Paper 555.
<http://docs.lib.purdue.edu/nanopub/555>

This document has been made available through Purdue e-Pubs, a service of the Purdue University Libraries. Please contact epubs@purdue.edu for additional information.

Physics of Carrier Backscattering in One- and Two-Dimensional Nanotransistors

Raseong Kim, *Student Member, IEEE*, and Mark S. Lundstrom, *Fellow, IEEE*

Abstract—The physics of carrier backscattering in 1-D and 2-D transistors is examined analytically and by numerical simulation. An analytical formula for the backscattering coefficient is derived for elastic scattering in a 1-D channel. This formula shows that the critical length for backscattering is somewhat longer than the kT length, and it depends on the shape of the channel potential profile. For inelastic scattering, Monte Carlo (MC) simulations show that the critical length is related to the phonon energy. The MC simulations also show that although the scattering physics in 1-D and 2-D transistors is very different, the overall backscattering characteristics are surprisingly similar. For an elastic process, this similarity is due to the compensating effects of the scattering rate and the fraction of scattered carriers, which contribute to the backscattering coefficient. For an inelastic process, the critical length is determined from the phonon energy for both 1-D and 2-D channels.

Index Terms—MOSFETs, nanowire (NW) transistor, scattering, semiconductor device modeling.

I. INTRODUCTION

SEMICONDUCTOR nanowire (NW) transistors are attracting attention as a possible solution to the scaling challenges of MOSFETs [1]–[6]. In addition to improved electrostatics, 1-D transistors provide novel characteristics due to quantum confinement [7], [8], which have been observed experimentally as the diameter scales down and the temperature (T_L) is lowered [9], [10]. A recent study of ballistic transistors shows, however, that except for differences in electrostatics, device performance metrics, such as the injection velocity and the intrinsic device delay, are similar for NW transistors and 2-D planar transistors, particularly at room temperature [11]. In the presence of scattering, however, one might expect the 1-D and 2-D transistors to behave differently due to dimension-dependent scattering [12], [13]. Our objective in this paper is to examine the physics of backscattering in 1-D and 2-D transistors.

The backscattering coefficient R in a field-free slab is expressed as [14]

$$R = \frac{L}{\lambda_0 + L} \quad (1)$$

Manuscript received May 12, 2008; revised September 29, 2008. Current version published December 19, 2008. This work was supported by the National Science Foundation under Grant ECS-0609282. The review of this paper was arranged by Editor C.-Y. Lu.

The authors are with the Network for Computational Nanotechnology, School of Electrical and Computer Engineering, Purdue University, West Lafayette, IN 47907 USA (e-mail: kim369@purdue.edu).

Color versions of one or more of the figures in this paper are available online at <http://ieeexplore.ieee.org>.

Digital Object Identifier 10.1109/TED.2008.2008368

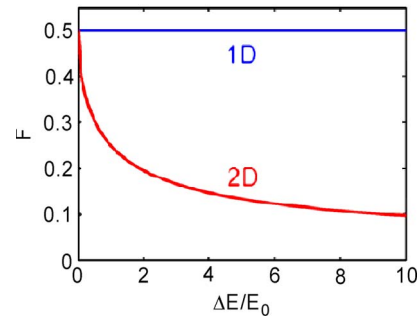


Fig. 1. Fraction (F) of backscattered carriers that contribute to R versus $\Delta E/E_0$ for 1-D and 2-D elastic/isotropic scattering.

where L is the channel length and λ_0 is the averaged backscattering mean free path under a low electric field (by low electric field, we mean that it is low enough to maintain near-equilibrium transport in the slab). It has been suggested that (1) can be generalized to high electric fields as [15]

$$R = \frac{l}{\lambda_0 + l} \approx \frac{L_{kT}}{\lambda_0 + L_{kT}} \quad (2)$$

where l is the critical length and L_{kT} (the “ kT length”) is the distance over which the potential drops by $k_B T_L/q$ [15] (by high electric field, we mean that the field produces off-equilibrium conditions for carriers in the slab). For inelastic scattering, it has been suggested that l is the distance from the top of the barrier to the point where carriers gain enough kinetic energy to emit optical phonons [16].

For planar devices, the critical region for backscattering occurs because the fraction F of the scattered carriers that contribute to R decreases as the carriers travel down the potential drop along the channel [17]. This occurs even for elastic scattering because only a small cone of backscattered carriers has sufficient kinetic energy to surmount the potential barrier and return to the source. This general understanding of backscattering has been extended by a number of recent studies [18]–[21]. Fischetti *et al.* [22] have, however, pointed out that long-range Coulomb effects could invalidate the concept of a critical length. This issue merits careful study but it is beyond the scope of this paper. The critical region for elastic backscattering in 1-D, however, may not apply because any carrier that backscatters has sufficient longitudinal momentum to surmount the barrier and return to the source. Fig. 1 shows a sketch of F versus $\Delta E/E_0$ for 1-D and 2-D elastic/isotropic scattering, where ΔE is the energy that a carrier gains and E_0 is the injection energy. For 2-D, F decreases steadily [17]; however,

F is constant at 0.5 for 1-D. This clear difference in F suggests that the backscattering characteristics may be different for 1-D and 2-D transistors.

In this paper, we perform analytical and numerical analyses to address the following questions: 1) “Is the concept of a critical length still valid in 1-D?” 2) “How is l related to L_{kT} ?” 3) “Does λ_0 control R even under high electric fields?” 4) “Does l change for elastic and inelastic scattering?” and 5) “How does the backscattering characteristic compare for 1-D and 2-D transistors?” Note that our objective in this paper is to provide “insight, not numbers” [23]. We use simple but physical model structures and scattering mechanisms to establish some general understanding that we believe will be broadly applicable.

This paper is organized as follows. In Section II, we assume a 1-D model device and analytically evaluate R for elastic/isotropic scattering. In Section III, the results from the analytical formula are compared with those from Monte Carlo (MC) simulations. The role of inelastic scattering in 1-D transistors is also studied through MC simulations. In Section IV, we repeat the analysis for a 2-D model device to compare backscattering physics in 1-D and 2-D. The conclusion follows in Section V.

II. ANALYTICAL TREATMENT OF BACKSCATTERING IN 1-D

In this section, an analytical formula for R is derived in 1-D, considering elastic/isotropic scattering. We define a 1-D model device (Section II-A) and assume a simple elastic scattering process (Section II-B). An analytical formula for R is derived using the one-flux method [24] for simple channel potential profiles (Section II-C). In [25], it was shown that (2), with $l = L_{kT}$, can be derived from the 1-D Boltzmann transport equation assuming a constant relaxation length. In that derivation, however, the authors assumed that the carrier velocity is constant at the thermal velocity in the current continuity condition. In our derivation, we consider the velocity variation along the channel, thereby improving on the previous derivation, as demonstrated by comparisons with numerical simulations in Section III.

A. Model Device

As a 1-D model device, we assume a rectangular silicon NW with 3-nm width (W) and [110] transport direction, where the electrons are confined in a 2-D box of width W . We consider only the lowest subband, i.e., a true 1-D transport. Then, the valley degeneracy (g_ν) is two, and we take the transverse effective mass of bulk silicon as the transport effective mass ($m^* = m_t$). Although the bulk effective mass is not exact for NWs [26], it should be useful for our simple model calculation. The schematic of the model device is shown in Fig. 2(a).

Although we treat only a single subband, it should be noted that intersubband scattering may become relevant under high drain bias when multisubbands are considered. Intersubband scattering mainly occurs between unprimed subbands [27], and it becomes more important as W or T_L increases. We expect, however, that intersubband scattering will not affect R significantly if it mostly occurs outside the critical region.

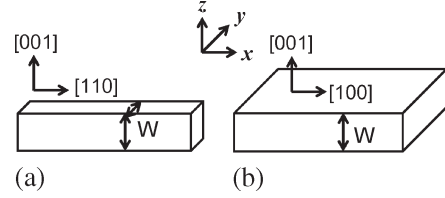


Fig. 2. (a) Schematic of the 1-D model device. The transport (x) direction is [110], and W is the width of the NW. (b) Schematic of the 2-D model device. The wafer orientation is (001), and W is the body thickness.

For our 1-D model device, the energy difference between the first and the second unprimed subbands is $3\hbar^2\pi^2/2m_lW^2 \sim 0.14$ eV, where the longitudinal electron effective mass m_l is $0.91m_0$. If this is less than the energy a carrier gains across the critical region, then we can roughly say that intersubband scattering is significant. We believe, however, that including intersubband scattering will not change the general conclusion of this paper. In Section IV, we consider a 2-D device with a large number of transverse modes, and the intermediate case of an NW with a few subbands (i.e., quasi-1-D transport) would not be substantially different from the two limiting cases we examine.

B. Elastic Scattering in 1-D

For elastic scattering, we assume intrasubband acoustic phonon scattering, which is elastic and isotropic near room temperature. The scattering rate due to acoustic phonon absorption/emission is

$$\frac{1}{\tau_{1-D}} = \frac{9\pi D_A^2 k_B T_L}{4g_\nu W^2 \hbar \rho v_S^2} g_{1-D} \quad (3)$$

where D_A is the electron acoustic deformation potential; ρ is the mass density; v_S is the sound velocity; and g_{1-D} is the 1-D density of states, with $g_{1-D} = 2g_\nu m^* / \pi \hbar \sqrt{2m^* E(p)}$, where $E(p)$ is the carrier kinetic energy. For a relaxation time in power-law form $\tau = \tau_0 (E(p)/k_B T_L)^s$ [28], the low-field mobility is $\mu = q\tau_0/m^* \times \Gamma(s + d/2 + 1)/\Gamma(d/2 + 1)$ in the nondegenerate limit, where d is the device dimensionality. The low-field mobility for our 1-D model device (μ_{1-D}) can be calculated using $d = 1$ and $s = 1/2$. From the 1-D Landauer formula [14], μ and λ_0 are related as $\mu = q/k_B T_L \times \lambda_0 v_T/2$, where v_T is the thermal velocity, with $v_T = \sqrt{2k_B T_L/\pi m^*}$. By equating this relation with μ_{1-D} , we obtain $\lambda_0 = 8W^2 \hbar^2 \rho v_S^2 / 9m^* D_A^2$, which is ~ 42 nm at $T_L = 300$ K for our model device with bulk silicon parameters [29]. One thing to note is that this λ_0 may be too large for a realistic NW transistor, where other scattering mechanisms, such as surface roughness scattering, play a significant role [30], [31].

C. Analytical Derivation of R

Let $V(x)$ be the potential profile along the channel. For elastic scattering, the carrier velocity at x is given as $v(x) = \sqrt{2(E_0 + qV(x))/m^*}$, where E_0 is the average energy of injected carriers. In the nondegenerate limit, E_0 is calculated to be $k_B T_L$ for 1-D because the distribution function of the carriers

injected in the x -direction is velocity weighted [28]. Then, the backscattering mean free path at x can be expressed as

$$\begin{aligned}\lambda(x) &= 2v(x)\tau_{1-D}(x) = \frac{8W^2\hbar^2\rho v_S^2}{9m^*D_A^2k_B T_L}(E_0 + qV(x)) \\ &= \lambda_0 \left(\frac{E_0 + qV(x)}{k_B T_L} \right).\end{aligned}\quad (4)$$

The factor of two appears in (4) because the scattering is isotropic. Then, the relation between the positively and negatively directed fluxes can be obtained from the one-flux method [24] as

$$\begin{aligned}\frac{d(n^+(x)v^+(x))}{dx} &= -\frac{n^+(x)v^+(x)}{\lambda(x)} + \frac{n^-(x)v^-(x)}{\lambda(x)} \\ &= -\frac{k_B T_L (n^+(x) - n^-(x)) v(x)}{\lambda_0 (E_0 + qV(x))}\end{aligned}\quad (5)$$

where n^+ and n^- represent the concentrations of positively and negatively moving carriers. In (5), it is assumed that the velocities of positively and negatively moving carriers are the same, as $v^+(x) = v^-(x) = v(x)$. From the current continuity condition, (5) becomes

$$\frac{d(n^+(x)v(x))}{dx} = -\frac{k_B T_L (n^+(0) - n^-(0)) v(0)}{\lambda_0 (E_0 + qV(x))}.\quad (6)$$

For a given $V(x)$, (6) may be integrated analytically to calculate R . Here, we consider two channel potential profiles, i.e., linear and parabolic potential profiles.

1) *Linear Potential*: For a linear potential profile, (6) becomes

$$\frac{d(n^+(x)v(x))}{dx} = -\frac{k_B T_L (n^+(0) - n^-(0)) v(0)}{\lambda_0 (E_0 + qE_x x)}\quad (7)$$

where E_x is the constant electric field along the x -direction. Using the boundary condition $n^-(L) = 0$ [25] and the current continuity $n^+(L)v(L) = (n^+(0) - n^-(0))v(0)$, (7) is integrated as

$$\begin{aligned}n^+(x)v(x) &= (n^+(0) - n^-(0)) v(0) \\ &\times \left(1 + \frac{k_B T_L}{\lambda_0 q E_x} \ln \left(\frac{E_0 + qE_x L}{E_0 + qE_x x} \right) \right).\end{aligned}\quad (8)$$

By evaluating (8) at $x = 0$ and rearranging the result, R is obtained as

$$R = \frac{n^-(0)}{n^+(0)} = \frac{L_{kT} \ln(1 + L/L_{kT})}{\lambda_0 + L_{kT} \ln(1 + L/L_{kT})}\quad (9)$$

where L_{kT} is defined as $L_{kT} = k_B T_L / qE_x$ [15].

In the low-field limit ($L \ll L_{kT}$), $L_{kT} \ln(1 + L/L_{kT}) \approx L$, and (9) reduces to $R \approx L/(\lambda_0 + L)$, as expected from (1). In the high-field limit, (9) has a similar form as (2); however, l is larger than L_{kT} and has a more complicated form which

depends on E_x and L , as $l = L_{kT} \ln(1 + L/L_{kT}) > L_{kT}$. The $1/R$ versus E_x relation obtained from (9) shows

$$\begin{aligned}\frac{1}{R} &= 1 + \frac{\lambda_0}{l} \\ &= 1 + \frac{\lambda_0 E_x}{k_B T_L / q \times \ln(1 + qE_x L / k_B T_L)} \\ &\simeq 1 + \frac{\lambda_0}{\Delta V} E_x\end{aligned}\quad (10)$$

where ΔV is the voltage drop across the critical region. It is observed that $1/R$ versus E_x is approximately linear with the slope of $\sim \lambda_0 / \Delta V$ because the E_x dependence in the log term is weak. Under a low electric field, ΔV is the total drain voltage. Under high electric fields, ΔV is somewhat larger than $k_B T_L / q$.

2) *Parabolic Potential*: For a given drain voltage V_d , the parabolic potential profile and L_{kT} are given as $V(x) = V_d x^2 / L^2$ and $L_{kT} = L \sqrt{k_B T_L / qV_d}$, respectively [25]. In a similar way to that used in the previous section, R is obtained as

$$R = \frac{L_{kT} \tan^{-1}(L/L_{kT})}{\lambda_0 + L_{kT} \tan^{-1}(L/L_{kT})}\quad (11)$$

and l can be defined as $l = L_{kT} \tan^{-1}(L/L_{kT})$. In the low-field limit ($V_d \ll k_B T_L / q$), $l \approx L$, and R reduces to the well-known low-field form in (1). Under high fields ($V_d \gg k_B T_L / q$), $l \approx L_{kT} \times \pi/2 > L_{kT}$, and $\Delta V = V_d / L^2 \times l^2 \sim V_d / L^2 \times \pi^2 L_{kT}^2 / 4 = \pi^2 / 4 \times k_B T_L / q$.

3) *Discussion*: Analytical formulas for R in (9) and (11) show that the concept of a critical length is still valid in 1-D. As shown in Fig. 1, once a carrier scatters elastically in a 1-D channel, it has a constant probability to go back to the source. The scattering rate, however, decreases as the carriers travel down the potential drop and gain kinetic energy [because the scattering rate is proportional to g_{1-D} , as given by (3)]; hence, the carriers have less chance to scatter deep inside the channel. Analytical formulas also show that λ_0 still controls R even under high electric fields. In addition, l is not as simple as expected from (2); it is a function of L_{kT} but it depends on L and the shape of the potential profile along the channel. For both linear and parabolic potential profiles, l is somewhat longer than L_{kT} under high electric fields. Finally, our derivation assumed that the velocities of positively and negatively moving carriers are the same. A simple MC simulator to be discussed in Section III-A shows that $v^-(0) \sim 0.9v^+(0)$, which indicates that our assumption is reasonable. More sophisticated MC simulations that treat multisubband scattering with a self-consistent channel potential have shown that $v^-(0) \sim 0.7v^+(0)$ [32]. The assumption of equal velocities for injected and backscattered carriers does not appear to affect our overall conclusions.

III. MC SIMULATION OF BACKSCATTERING IN 1-D

In this section, the implementation of the MC simulator is explained (Section III-A), and the results for R from analytical formulas derived in Section II are compared with those from

MC simulations (Section III-B). Then, the role of inelastic scattering in 1-D transistors is studied through MC simulations (Section III-C).

A. MC Simulator

The MC simulator takes the incident-flux approach, assuming nondegenerate contacts [28]. Carrier degeneracy may affect the backscattering characteristics [20]; however, it is beyond the scope of this paper. The simulation begins with a carrier selected at random from the flux injected from the source contact ($x = 0$). The carrier is followed until it comes back to the source or reaches the drain contact ($x = L$) under $-x$ -directed electric fields. For 1-D, carriers are allowed to move only along the x -direction, while the carriers in 2-D simulation also have momentum along the y -direction. We assume that the carriers that reach contacts simply exit the channel [28]. When the carrier injection from the drain contact is turned off [25], R can be calculated by dividing the number of carriers returning to the source by the total number of carriers injected from the source contact. The potential profile along the channel is fixed to explore how the shape of the potential profile affects R and to compare against the analytical results of Section II.

The physics and simulations of carrier scattering in NWs constitute an active area of research [12], [33], [34]. To quantitatively simulate NW transistors, various scattering processes, such as confined phonon scattering [35], surface roughness scattering [30], [31], and intersubband scattering [27], should be considered. In this paper, however, we use simple but physical model scattering mechanisms, treating only a single subband to understand the general principles for elastic and inelastic backscatterings. For elastic scattering, as discussed in Section II, we assume that the scattering rate is proportional to the density of states and the parameters are taken from the intrasubband acoustic phonon scattering for bulk silicon [29]. For inelastic scattering, we assume intervalley phonon scattering with bulk silicon parameters [29].

B. Comparison With the Analytical Formula

As shown in (1), $1/T$ versus L is linear under low electric fields, as $1/T = 1 + L/\lambda_0$. From $1/T$ versus L obtained from MC simulations with $E_x = 10$ V/cm at $T_L = 300$ K, λ_0 is extracted to be ~ 38 nm, which is in a good agreement with the analytical result (~ 42 nm). Fig. 3(a) shows a comparison of the R versus E_x results from the analytical formula in (9) with the MC simulation results. The analytical and numerical results match very well for both low and high electric fields. The analytical formula for the parabolic potential profile in (11) also agrees well with the MC simulation result, as shown in Fig. 3(b).

Fig. 4 shows the analytical and MC simulation results for $1/R$ versus E_x under high electric fields. The l for each E_x can be extracted using $1/R = 1 + \lambda_0/l$, and the result is shown as the inset of Fig. 4. As expected from (10), although $1/R$ versus E_x looks quite linear, the l/L_{kT} ratio is not constant but increases with E_x . Fig. 4 also shows that l is a few times longer

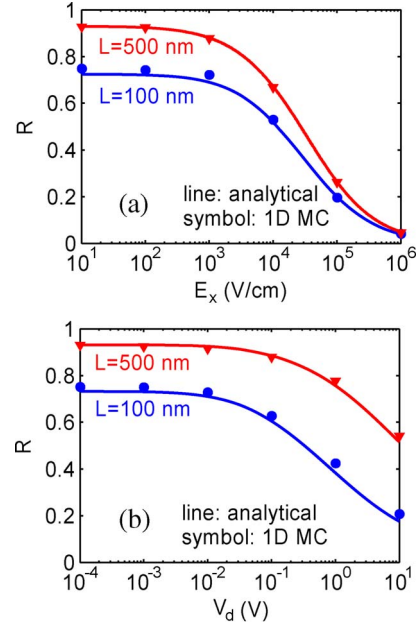


Fig. 3. Comparison of the analytical formulas for R and MC simulation results considering elastic/isotropic scattering in the 1-D model device, with $L = 100$ nm/500 nm at $T_L = 300$ K. (a) R versus E_x obtained from the (line) analytical formula and the (symbol) MC simulation for linear channel potentials. (b) R versus V_d from the (line) analytical formula and the (symbol) MC simulation for parabolic potential profiles.

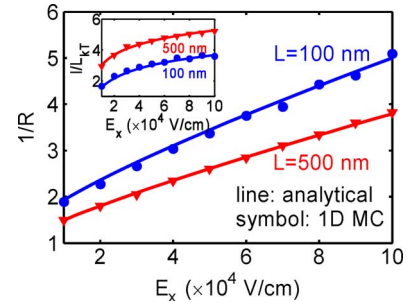


Fig. 4. (Symbol) MC simulation results for $1/R$ versus E_x (linear potential) for the 1-D model device and (line) comparison with the analytical results, with $L = 100$ nm/500 nm at $T_L = 300$ K. (Inset) l/L_{kT} versus E_x from the (symbol) MC simulation and (line) analytical formula.

than L_{kT} and depends on L , as $l \approx 2 \sim 4L_{kT}$ for $L = 100$ nm and $l \approx 3 \sim 5L_{kT}$ for $L = 500$ nm.

Let n_{BS} and x_{max} be, respectively, the number of backscattered carriers that return to the source and the maximum distance that each backscattered carrier had reached before returning to the source. Then, F can be estimated from the MC simulation results by dividing n_{BS} versus x_{max} by the total number of scattering events at each point x . As shown in Fig. 5, F for 1-D is quite uniform along the channel and close to 0.5, as expected analytically. It is mostly less than 0.5 because some of the carriers that backscatter scatter again and do not return to the source.

C. Inelastic Scattering in 1-D

For inelastic scattering, we assume g -type intervalley scattering with bulk silicon parameters [29]. For this scattering

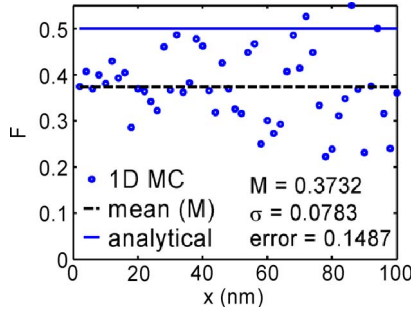


Fig. 5. F versus x estimated from the (symbol) MC simulation and the (solid line) analytical formula for the 1-D model device, with $L = 100$ nm and $E_x = 10^5$ V/cm (linear potential) at $T_L = 300$ K. M and σ are the mean and the standard deviation of the MC simulation result, respectively. M is shown as a dashed line. The error is estimated by taking the root mean square of the difference between the analytical and the simulation results.

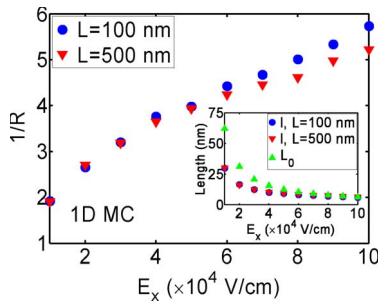


Fig. 6. MC simulation results for $1/R$ versus E_x (linear potential) for the 1-D model device, with $L = 100$ nm/500 nm at $T_L = 300$ K, considering elastic and inelastic scattering mechanisms. (Inset) MC simulation results for l versus E_x and comparison with $L_0 = \hbar\omega_o/E_x$, where $\hbar\omega_o$ is the LO phonon energy.

process, there are three phonon modes, namely, transverse acoustic, longitudinal acoustic, and longitudinal optical (LO) [29]. Due to the large momentum change and the almost constant phonon energy, intervalley phonon scattering is usually treated in the same way as optical phonon scattering [29]. Then, the scattering rate due to absorption and emission of each intervalley phonon becomes

$$\frac{1}{\tau_{1-D}} = \frac{9\pi D_{if}^2}{8g_\nu W^2 \rho \omega_{if}} \left(N_i + \frac{1}{2} \mp \frac{1}{2} \right) g_{1-D}(E \pm \hbar\omega_{if}) \quad (12)$$

where D_{if} is the intervalley deformation potential, N_i is the number of phonons, and $\hbar\omega_{if}$ is the intervalley phonon energy.

Fig. 6 shows the MC simulation results for $1/R$ versus E_x , considering both elastic and inelastic scattering mechanisms for linear potential profiles. We observe that $1/R$ increases with E_x as it did in the elastic scattering case; however, the slope rolls off as E_x increases. It has been suggested that l is the distance over which the potential drops by the optical phonon energy for the inelastic scattering process [16]. Among the three inelastic scattering processes, the LO process is dominant due to the high D_{if} . Hence, we define $L_0 = \hbar\omega_o/E_x$, where $\hbar\omega_o$ is the LO phonon energy, with $\hbar\omega_o = 0.062$ eV [29]. For our model device at room temperature, the intravalley acoustic phonon and the LO processes are the two dominant scattering mechanisms. As shown in the inset of Fig. 6, l decreases with increasing E_x and finally approaches L_0 . Under relatively low electric fields, L_0 is long, and l is mainly controlled by elastic scattering near

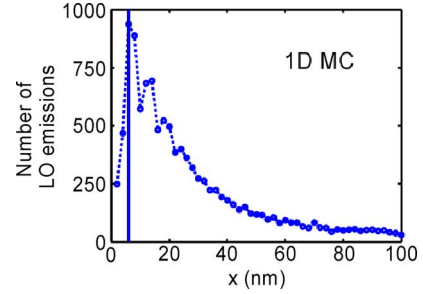


Fig. 7. MC simulation results for the number of LO emissions versus x for the 1-D model device, with $L = 100$ nm and $E_x = 10^5$ V/cm (linear potential) at $T_L = 300$ K. The slab size is 2 nm. (Bar) l coincides with the position where the LO emission is peaked.

the source region. As E_x increases, the optical phonon process starts to dominate and l becomes $\sim L_0$ because the carriers gain enough energy to emit optical phonons near the source. Fig. 7 shows that the critical length coincides with the position where LO emission is peaked. This means that once a carrier passes through the critical region, it is hard for the carrier to go back to the source because the carrier loses energy due to phonon emission.

IV. BACKSCATTERING IN 2-D

In this section, we discuss the scattering physics of 2-D transistors and how it differs from the 1-D case. We define a 2-D model device (Section IV-A) and discuss MC simulation results for elastic (Section IV-B) and inelastic (Section IV-C) processes.

A. Model Device

As a 2-D model device, we assume a silicon thin body with $W = 3$ nm with (001) wafer, and the electrons are confined in a 1-D box of width W . Only the lowest subband is considered, with $g_\nu = 2$ and $m^* = m_t$. The device schematic is shown in Fig. 2(b).

B. Elastic Scattering in 2-D

In a similar approach used for the 1-D model device, we assume intrasubband acoustic phonon scattering. Then, the scattering rate due to acoustic phonon absorption/emission becomes

$$\frac{1}{\tau_{2-D}} = \frac{3\pi D_A^2 k_B T_L}{2g_\nu W \hbar \rho v_S^2} g_{2-D} \quad (13)$$

where g_{2-D} is the 2-D density of states, with $g_{2-D} = g_\nu m^* / \pi \hbar^2$. Then, λ_0 is calculated as ~ 104 nm at $T_L = 300$ K using bulk silicon parameters [29]. As it was for the 1-D case, this λ_0 may be too large for a realistic 2-D transistor because our model treats phonon scattering only. The result extracted from the MC simulation is ~ 93 nm, which is consistent with the analytical estimation. We note that λ_0 for 1-D in Section II is shorter than that for 2-D. This is due to the increased electron-phonon wave function overlap that compensates for the effect of the reduced density of states in 1-D [12].

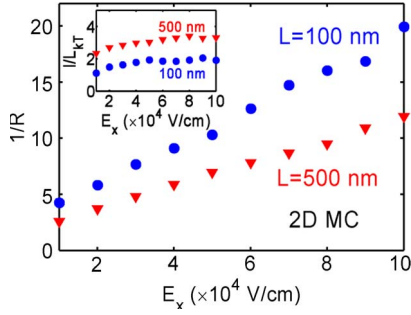


Fig. 8. MC simulation results for $1/R$ versus E_x (linear potential) for the 2-D model device, with $L = 100$ nm/500 nm at $T_L = 300$ K, considering elastic scattering. (Inset) l/L_{kT} versus E_x from the MC simulation.

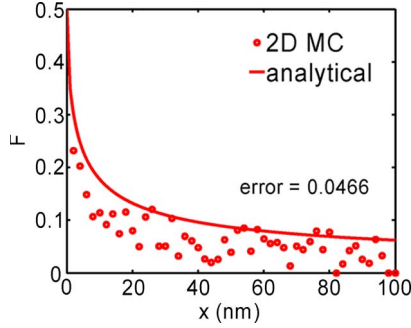


Fig. 9. F versus x from the (symbol) MC simulation and the (line) analytical formula for the 2-D model device, with $L = 100$ nm and $E_x = 10^5$ V/cm (linear potential) at $T_L = 300$ K. The error is estimated by taking the root mean square of the difference between the analytical and the simulation results.

Fig. 8 shows MC simulation results for $1/R$ versus E_x for the 2-D model device. The relation between $1/R$ and E_x looks linear as it did in 1-D, and we observe similar E_x and L dependences of l . The l/L_{kT} ratio increases with E_x ; $l \sim 2L_{kT}$ for $L = 100$ nm, and $l \sim 3L_{kT}$ for $L = 500$ nm. These critical lengths are shorter than those of 1-D but are still longer than L_{kT} . In Fig. 9, F from the MC simulation is compared with the analytical result [17]

$$F = \frac{\cos^{-1} \left(\sqrt{\Delta E / (\Delta E + E_0)} \right)}{\pi} \quad (14)$$

where $\Delta E = qE_x x$ for the linear channel potential. As expected, F decreases steadily as the carrier moves down the potential drop.

Observations in Fig. 8 seem to show that backscattering characteristics in 1-D and 2-D are similar. To determine why it is so, we artificially increase D_A for 2-D to make λ_0 the same for 1-D and 2-D. Then, R is the same for 1-D and 2-D under low electric fields; however, we might observe some difference under high electric fields. As shown in Fig. 10, however, backscattering characteristics are very similar even under high electric fields. This is surprising because 1-D and 2-D transistors have distinctively different characteristics for F and scattering rates.

The similar backscattering characteristics in 1-D and 2-D elastic scattering can be understood in the following way. If we assume that a backscattered carrier propagates to the

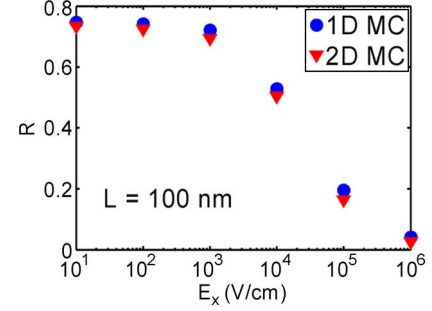


Fig. 10. MC simulation results for R versus E_x (linear potential) for 1-D and 2-D model devices, with $L = 100$ nm at $T_L = 300$ K. The acoustic deformation potential for 2-D has been artificially increased to make λ_0 the same for 1-D and 2-D.

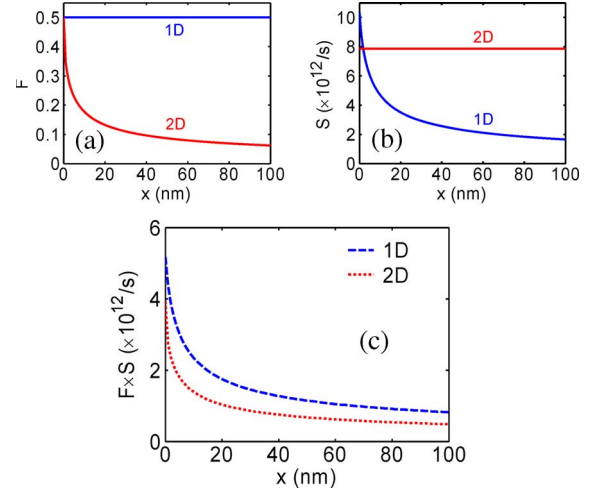


Fig. 11. Analytical estimates for (a) F versus x , (b) S versus x , and (c) $F \times S$ versus x for 1-D and 2-D transistors, with $L = 100$ nm and $E_x = 10^5$ V/cm (linear potential) at $T_L = 300$ K, where S is the scattering rate.

source without subsequent scattering, then R can be simply estimated as

$$R \sim \int_0^L dx \frac{F(x)S(x)}{v(x)} \quad (15)$$

where $F(x)$ is the fraction shown in Fig. 1 and $S(x)$ is the scattering rate in (3) or (13). Although $F(x)$ and $S(x)$ are very different for 1-D and 2-D transistors, their product $F(x)S(x)$ looks very similar, as shown in Fig. 11. Due to these compensating effects of $F(x)$ and $S(x)$, R behaves similarly in 1-D and 2-D transistors.

Fig. 11 also explains why the critical lengths for 2-D transistors are shorter than those for 1-D. As shown in Fig. 11(c), $F(x)S(x)$ near the source decreases more rapidly in 2-D than in 1-D, indicating a shorter l for 2-D. This is because $F(x)$ for 2-D drops more rapidly than $S(x)$ for 1-D does, as shown in Fig. 11(a) and (b). The sharp decrease of $F(x)$ for 2-D comes from (14), which is derived from the fact that only a small fraction of backscattered carriers has sufficient longitudinal momentum to return to the source due to the scattering into transverse momentum states [17]. Therefore, we believe that

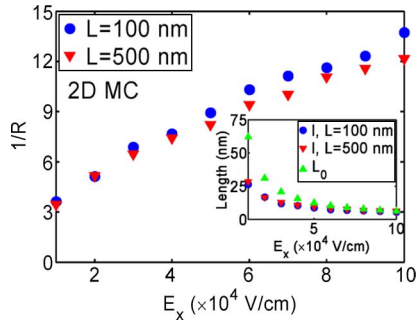


Fig. 12. MC simulation results for $1/R$ versus E_x (linear potential) for the 2-D model device, with $L = 100$ nm at $T_L = 300$ K. (Inset) MC simulation results for l versus E_x and comparison with $L_0 = \hbar\omega_o/E_x$, where $\hbar\omega_o$ is the LO phonon energy.

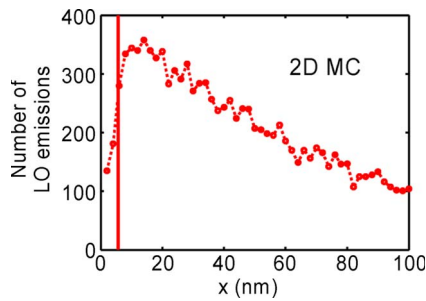


Fig. 13. MC simulation results for the number of LO emissions versus x for the 2-D model device, with $L = 100$ nm and $E_x = 10^5$ V/cm (linear potential) at $T_L = 300$ K. The slab size is 2 nm. (Bar) l falls near the position where LO emission is peaked.

the shorter critical lengths for 2-D are due to the scattering into transverse momentum states.

C. Inelastic Scattering in 2-D

As in the 1-D analysis, we assume g -type intervalley scattering for inelastic scattering. Fig. 12 shows the MC simulation results for $1/R$ versus E_x . Similar to the 1-D case, the $1/R$ versus E_x slope rolls off, and l approaches L_0 as E_x increases. In Fig. 13, l is close to the distance from the source to the position where LO emission is peaked, although a little shorter. This is because l is determined by combining the critical lengths due to the two dominant scattering mechanisms, namely, the elastic acoustic phonon (l_{ac}) and the inelastic (L_0) processes. Between the two, the shorter one dominates. As discussed in Section IV-B, l_{ac} is shorter in 2-D than in 1-D; hence, the shorter l_{ac} in 2-D has a larger effect on the resulting l . Therefore, l in 2-D is a little shorter than L_0 while it is close to L_0 for 1-D, as shown in Fig. 7.

V. CONCLUSION

In this paper, we examined the concept of a critical length for backscattering in 1-D transistors, considering elastic and inelastic scattering mechanisms. We also compared the scattering physics in 1-D and 2-D transistors using MC simulations. We showed that the concept of a critical length is still valid for elastic scattering in 1-D. Our theoretical expression for the backscattering coefficient, which was confirmed

by MC simulations, shows that the backscattering coefficient depends on the kT length; however, the critical length is somewhat greater than the kT length, and it also depends on the potential profile in the channel. The analytical expression also showed that backscattering is controlled by the near-equilibrium mean free path even under high electric fields. The role of inelastic scattering was studied using MC simulations, and the results support the work of [15]; the critical length for inelastic scattering is related to the phonon energy. Finally, we showed that backscattering coefficients in 2-D behave very similarly to those in 1-D. For elastic scattering, this similarity is explained in terms of the compensating effects of the scattering rate and the fraction of scattered carriers that contribute to the backscattering coefficient. For inelastic scattering, the critical length is determined by the phonon energy for both 1-D and 2-D.

ACKNOWLEDGMENT

The authors would like to thank the Network for Computational Nanotechnology, supported by the National Science Foundation under cooperative agreement EEC-0634750, for providing computational support, and C. Jeong at Purdue University, West Lafayette, IN, for the helpful discussions.

REFERENCES

- [1] *International Technology Roadmap for Semiconductors*, 2007, Semicond. Ind. Assoc. [Online]. Available: <http://www.itrs.net>
- [2] S. D. Suk, S.-Y. Lee, S.-M. Kim, E.-J. Yoon, M.-S. Kim, M. Li, C. W. Oh, K. H. Yeo, S. H. Kim, D.-S. Shin, K.-H. Lee, H. S. Park, J. N. Han, C. J. Park, J.-B. Park, D.-W. Kim, D. Park, and B.-I. Ryu, "High performance 5 nm radius twin silicon nanowire MOSFET (TSNWFET): Fabrication on bulk Si wafer, characteristics, and reliability," in *IEDM Tech. Dig.*, Washington, DC, Dec. 2005, pp. 717–720.
- [3] N. Singh, A. Agarwal, L. K. Bera, T. Y. Liow, R. Yang, S. C. Rustagi, C. H. Tung, R. Kumar, G. Q. Lo, N. Balasubramanian, and D. L. Kwong, "High-performance fully depleted silicon nanowire (diameter ≤ 5 nm) gate-all-around CMOS devices," *IEEE Electron Device Lett.*, vol. 27, no. 5, pp. 383–386, May 2006.
- [4] N. Singh, F. Y. Lim, W. W. Fang, S. C. Rustagi, L. K. Bera, A. Agarwal, C. H. Tung, K. M. Hoe, S. R. Omampuliyur, D. Tripathi, A. O. Adeyeye, G. Q. Lo, N. Balasubramanian, and D. L. Kwong, "Ultra-narrow silicon nanowire gate-all-around CMOS devices: Impact of diameter, channel-orientation and low temperature on device performance," in *IEDM Tech. Dig.*, San Francisco, CA, Dec. 2006, pp. 547–550.
- [5] K. H. Yeo, S. D. Suk, M. Li, Y.-Y. Yeoh, K. H. Cho, K.-H. Hong, S. Yun, M. S. Lee, N. Cho, K. Lee, D. Hwang, B. Park, D.-W. Kim, D. Park, and B.-I. Ryu, "Gate-all-around (GAA) twin silicon nanowire MOSFET (TSNWFET) with 15 nm length gate and 4 nm radius nanowires," in *IEDM Tech. Dig.*, San Francisco, CA, Dec. 2006, pp. 539–542.
- [6] K. H. Cho, K. H. Yeo, Y. Y. Yeoh, S. D. Suk, M. Li, J. M. Lee, M. S. Kim, D. W. Kim, D. Park, B. H. Hong, Y. C. Jung, and S. W. Hwang, "Experimental evidence of ballistic transport in cylindrical gate-all-around twin silicon nanowire metal-oxide-semiconductor field-effect transistors," *Appl. Phys. Lett.*, vol. 92, no. 5, pp. 052102–052103, Feb. 2008.
- [7] J. P. Colinge, W. Xiong, C. R. Cleavelin, T. Schulz, K. Schrufer, K. Matthews, and P. Patruno, "Room-temperature low-dimensional effects in Pi-gate SOI MOSFETs," *IEEE Electron Device Lett.*, vol. 27, no. 9, pp. 775–777, Sep. 2006.
- [8] R. Kim and M. S. Lundstrom, "Characteristic features of one-dimensional ballistic transport in nanowire MOSFETs," *IEEE Trans. Nanotechnol.*, 2008. [Online]. Available: http://ieeexplore.ieee.org/xpls/pre_abs_all.jsp?arnumber=4468038
- [9] K. H. Cho, S. D. Suk, Y. Y. Yeoh, M. Li, K. H. Yeo, D.-W. Kim, S. W. Hwang, D. Park, and B.-I. Ryu, "Observation of single electron tunneling and ballistic transport in twin silicon nanowire MOSFETs

- (TSNWFETs) fabricated by top-down CMOS process," in *IEDM Tech. Dig.*, San Francisco, CA, Dec. 2006, pp. 543–546.
- [10] S. C. Rustagi, N. Singh, Y. F. Lim, G. Zhang, S. Wang, G. Q. Lo, N. Balasubramanian, and D. L. Kwong, "Low-temperature transport characteristics and quantum-confinement effects in gate-all-around Si-nanowire n-MOSFET," *IEEE Electron Device Lett.*, vol. 28, no. 10, pp. 909–912, Oct. 2007.
- [11] R. Kim, N. Neophytou, A. Paul, G. Klimeck, and M. S. Lundstrom, "Dimensionality in metal-oxide-semiconductor field-effect transistors: A comparison of one-dimensional and two-dimensional ballistic transistors," *J. Vac. Sci. Technol. B, Microelectron. Process. Phenom.*, vol. 26, no. 4, pp. 1628–1631, Aug. 2008.
- [12] R. Kotlyar, B. Obradovic, P. Matagne, M. Stettler, and M. D. Giles, "Assessment of room-temperature phonon-limited mobility in gated silicon nanowires," *Appl. Phys. Lett.*, vol. 84, no. 25, pp. 5270–5272, Jun. 2004.
- [13] S. O. Koswatta, S. Hasan, M. S. Lundstrom, M. P. Anantram, and D. E. Nikonov, "Nonequilibrium Green's function treatment of phonon scattering in carbon-nanotube transistors," *IEEE Trans. Electron Devices*, vol. 54, no. 9, pp. 2339–2351, Sep. 2007.
- [14] S. Datta, *Electronic Transport in Mesoscopic Structures*. Cambridge, U.K.: Cambridge Univ. Press, 1995.
- [15] M. Lundstrom, "Elementary scattering theory of the Si MOSFET," *IEEE Electron Device Lett.*, vol. 18, no. 7, pp. 361–363, Jul. 1997.
- [16] K. Natori, "Ballistic MOSFET reproduces current-voltage characteristics of an experimental device," *IEEE Electron Device Lett.*, vol. 23, no. 11, pp. 655–657, Nov. 2002.
- [17] M. Lundstrom and Z. Ren, "Essential physics of carrier transport in nanoscale MOSFETs," *IEEE Trans. Electron Devices*, vol. 49, no. 1, pp. 133–141, Jan. 2002.
- [18] P. Palestri, D. Esseni, S. Eminent, C. Fiegna, E. Sangiorgi, and L. Selmi, "A Monte-Carlo study of the role of scattering in decanometer MOSFETs," in *IEDM Tech. Dig.*, San Francisco, CA, Dec. 2004, pp. 605–608.
- [19] P. Palestri, D. Esseni, S. Eminent, C. Fiegna, E. Sangiorgi, and L. Selmi, "Understanding quasi-ballistic transport in nano-MOSFETs: Part I—Scattering in the channel and in the drain," *IEEE Trans. Electron Devices*, vol. 52, no. 12, pp. 2727–2735, Dec. 2005.
- [20] P. Palestri, R. Clerc, D. Esseni, L. Lucci, and L. Selmi, "Multi-subband-Monte-Carlo investigation of the mean free path and of the kT layer in degenerated quasi ballistic nanoMOSFETs," in *IEDM Tech. Dig.*, San Francisco, CA, Dec. 2006, pp. 945–948.
- [21] K. Natori, "Ballistic/quasi-ballistic transport in nanoscale transistor," *Appl. Surf. Sci.*, vol. 254, no. 19, pp. 6194–6198, Jul. 2008.
- [22] M. V. Fischetti, T. P. O'Regan, N. Sudarshan, C. Sachs, J. Seonghoon, K. Jiseok, and Z. Yan, "Theoretical study of some physical aspects of electronic transport in nMOSFETs at the 10-nm gate-length," *IEEE Trans. Electron Devices*, vol. 54, no. 9, pp. 2116–2136, Sep. 2007.
- [23] R. W. Hamming, *The Art of Doing Science and Engineering: Learning to Learn*. Amsterdam, The Netherlands: Gordon and Breach, 1997.
- [24] J. P. McKelvey, R. L. Longini, and T. P. Brody, "Alternative approach to the solution of added carrier transport problems in semiconductors," *Phys. Rev.*, vol. 123, no. 1, pp. 51–57, Jul. 1961.
- [25] R. Clerc, P. Palestri, and L. Selmi, "On the physical understanding of the kT -layer concept in quasi-ballistic regime of transport in nanoscale devices," *IEEE Trans. Electron Devices*, vol. 53, no. 7, pp. 1634–1640, Jul. 2006.
- [26] J. Wang, A. Rahman, A. Ghosh, G. Klimeck, and M. Lundstrom, "On the validity of the parabolic effective-mass approximation for the I - V calculation of silicon nanowire transistors," *IEEE Trans. Electron Devices*, vol. 52, no. 7, pp. 1589–1595, Jul. 2005.
- [27] S. Jin, M. V. Fischetti, and T.-W. Tang, "Differential conductance fluctuations in silicon nanowire transistors caused by quasiballistic transport and scattering induced intersubband transitions," *Appl. Phys. Lett.*, vol. 92, no. 8, p. 082103-3, Feb. 2008.
- [28] M. S. Lundstrom, *Fundamentals of Carrier Transport*, 2nd ed. Cambridge, U.K.: Cambridge Univ. Press, 2000.
- [29] C. Jacoboni and L. Reggiani, "The Monte Carlo method for the solution of charge transport in semiconductors with applications to covalent materials," *Rev. Mod. Phys.*, vol. 55, no. 3, pp. 645–705, Jul. 1983.
- [30] J. Wang, E. Polizzi, A. Ghosh, S. Datta, and M. Lundstrom, "Theoretical investigation of surface roughness scattering in silicon nanowire transistors," *Appl. Phys. Lett.*, vol. 87, no. 4, pp. 043101–043103, Jul. 2005.
- [31] S. Jin, M. V. Fischetti, and T.-W. Tang, "Modeling of electron mobility in gated silicon nanowires at room temperature: Surface roughness scattering, dielectric screening, and band nonparabolicity," *J. Appl. Phys.*, vol. 102, no. 8, pp. 083715–083714, Oct. 2007.
- [32] H. Tsuchiya, K. Fujii, T. Mori, and T. Miyoshi, "A quantum-corrected Monte Carlo study on quasi-ballistic transport in nanoscale MOSFETs," *IEEE Trans. Electron Devices*, vol. 53, no. 12, pp. 2965–2971, Dec. 2006.
- [33] S. Jin, Y. J. Park, and H. S. Min, "A three-dimensional simulation of quantum transport in silicon nanowire transistor in the presence of electron-phonon interactions," *J. Appl. Phys.*, vol. 99, no. 12, pp. 123710–123719, Jun. 2006.
- [34] E. B. Ramayya, D. Vasileska, S. M. Goodnick, and I. Knezevic, "Electron mobility in silicon nanowires," *IEEE Trans. Nanotechnol.*, vol. 6, no. 1, pp. 113–117, Jan. 2007.
- [35] L. Donetti, F. Gamiz, J. B. Roldan, and A. Godoy, "Acoustic phonon confinement in silicon nanolayers: Effect on electron mobility," *J. Appl. Phys.*, vol. 100, no. 1, pp. 013701–013707, Jul. 2006.



Raseong Kim (S'09) received the B.S. degree in electrical engineering and the M.S. degree in electrical engineering and computer science from Seoul National University, Seoul, Korea, in 2003 and 2005, respectively. She is currently working toward the Ph.D. degree in electrical and computer engineering in the School of Electrical and Computer Engineering, Purdue University, West Lafayette, IN.

Her current research interests include device physics and simulations of low-dimensional nanoscale devices.



Mark S. Lundstrom (S'72–M'74–SM'80–F'94) received the B.E.E. and M.S.E.E. degrees from the University of Minnesota, Minneapolis, in 1973 and 1974, respectively, and the Ph.D. degree in electrical engineering from Purdue University, West Lafayette, IN, in 1980.

From 1974 to 1977, he was with Hewlett-Packard Corporation, Loveland, CO, where he worked on integrated circuit process development and on manufacturing support. He is with Purdue University, where, since 1980, he has been with School of Electrical Engineering, Purdue University, as the Founding Director of the Network for Computational Nanotechnology and, currently, as the Don and Carol Scifres Distinguished Professor of electrical and computer engineering; he was, from 1989 to 1993, the Director of the Optoelectronics Research Center and was, from 1991 to 1994, the Assistant Dean of Engineering. His current research interest includes physics of small electronic devices, particularly nanoscale transistors and carrier transport in semiconductor devices.

Prof. Lundstrom currently serves as an IEEE Electron Devices Society Distinguished Lecturer. He is a Fellow of the American Physical Society and of the American Association for the Advancement of Science. In 1992, he was the recipient of the Frederick Emmons Terman Award from the American Society for Engineering Education. With his colleague, S. Datta, he was awarded the 2002 IEEE Cleo Brunetti award for their work on nanoscale electronic devices. In the same year, they shared the Semiconductor Research Corporation's Technical Excellence Award. In 2005, he was the recipient of the Semiconductor Industry Association's University Researcher Award for his career contributions to the physics and simulation of semiconductor devices. Most recently, in 2006, he received the IEEE Electron Devices Society's Education Award.

Most recently, in 2006, he received the IEEE Electron Devices Society's Education Award.